

PHOTOGRAMMETRY AND COMPUTER GRAPHICS FOR VISUAL IMPACT ANALYSIS IN ARCHITECTURE

Peter Durisch
Informatik im Ingenieurwesen, ETH-Hoenggerberg
CH-8093 Zurich, Switzerland
e-mail: durisch@pfi.ethz.ch
ISPRS Commission V

ABSTRACT :

The paper presents a method to produce realistic computer-generated color images which aids to the judgement of aesthetic properties of planned buildings. The planned buildings are embedded into the existing environment by photomontage. The planar universe of conventional photomontaging is extended to three dimensions. During an interactive preprocessing step, a three-dimensional description of the existing environment is created: Geometrical data, atmospheric parameters and illumination parameters are retrieved from digital site photographs. The final image, combining the planned building and the environment represented by the site photographs, is rendered by an extended ray-tracing algorithm. The algorithm operates in three-dimensional object space and handles the interaction between the building and its environment with respect to hiding, shadowing and interreflection. For the simulation of illumination effects, material parameters are retrieved from the photographs at rendering time.

KEY WORDS : Image Synthesis, Ray-tracing, Image Analysis, Feature Measurement, Visual Impact Analysis.

1. INTRODUCTION

Among the traditional methods which support the delicate job of judging the visual impact of planned buildings on the landscape or cityscape are: images (plans, perspective drawings, photomontages) and three-dimensional hand-crafted models. Though there is a justification for all of these, observation reveals that they are either unable to show the subtle effects which make up the overall appearance of a building, inflexible for case studies, or expensive due to the invested manual and artistic work. Thus, finding new methods to provide accurate sources with which to judge the aesthetic properties of planned buildings seems to be a worthy goal.

A fundamental requirement is that a building needs to be integrated into the existing environment (landscape, cityscape) (Leonhardt, 1984). The paper presents a method to produce realistic computer-generated color images which aids to the judgement of aesthetic properties of planned buildings. The planned buildings are embedded into the existing environment by photomontage. Photomontage is the combination of artificial objects (the planned building) with a particular environment represented by a number of digital site photographs. During an interactive preprocessing step, a three-dimensional description of the environment is retrieved from the photographs. In a second step, the photographs, the information retrieved from the photographs and the CAD model of the building are used to generate the final images. These show the planned building embedded in the existing environment from the perspectives of the site photographs. See also Durisch (Durisch, 1992).

2. PREVIOUS WORK

Computer-generated objects overlaid on background photographs are shown by Uno & Matsuka (Uno, 1979), Feibush et al. (Feibush, 1980), (BDC, 1990), Takagi et al. (Takagi, 1990) and Doi et al. (Doi, 1991). Maver et al. (Maver, 1985) calculate the camera's position and orientation in three-dimensional object space. The wireframe model of the planned

building is perspectively mapped onto the background photograph and an artist completes the drawing within the frame. Background objects hidden by the building are manually eliminated from the photograph. Then the corrected photograph is transparently overlaid onto the image of the building. Nakamae et al. (Nakamae, 1986) calculate the camera's position and orientation in object space and retrieve atmospheric parameters and illumination parameters from the photograph. The image of the building is generated by considering the retrieved information and overlaid onto the background photograph. Finally, it is covered by the manually identified foreground. The approximation of the background scene by faces and polyhedra in object space allows to generate shadows and to simulate various atmospheric conditions. Object space coordinates are obtained from topographical maps. Terzopoulos & Witkin (Terzopoulos, 1988) show an animation with deformable solid objects copied into a real background scene which was approximated by planar faces in object space.

Kaneda et al. (Kaneda, 1989) generate a three-dimensional terrain model from cartographical data. The surface texture of the model is derived from aerial photographs. Artificial objects are merged with the terrain by a method of Nakamae et al. (Nakamae, 1989) for the combination of a foreground and a background based on known depth information. Though the three-dimensional terrain model allows any observer position, the approach is of limited use whenever details of the environment, especially those visible in horizontal views, are required. Thirion (Thirion, 1992) generates images for the test of image processing algorithms. A three-dimensional model of an existing building is retrieved photogrammetrically from aerial photographs. The surface texture of the model is derived from the same photographs. The three-dimensional model allows any observer position if the geometry of the scene is known with sufficient precision and if photographs from suitable perspectives are available. Changes in illumination are simulated by removing and adding shadows. For this purpose, illumination parameters and material parameters are retrieved from the given photographs.

3. MODELS

Models serve to simplify the description of some aspects of the physical world. This section introduces important radiometric quantities and models for the representation of light sources, materials, geometrical objects and the camera as well as models for the simulation of atmospheric effects and illumination effects.

3.1 Radiometric Quantities

Irradiance $E = d\Phi / dF$ [Wm^{-2}] at a point on a surface element is the radiant power $d\Phi$ [W] incident on the surface element, divided by the area dF [m^{-2}] of the surface element. **Radiance** $L = d^2\Phi / (\cos\theta dF d\omega)$ [$Wm^{-2}sr^{-1}$] at a point on a surface element and in a given direction \hat{l} is the radiant power $d\Phi$ incident on the surface element or leaving the surface element in a cone containing \hat{l} , divided by the solid angle $d\omega$ [sr] of that cone and the projected area $\cos\theta dF = \hat{n} \cdot \hat{l} dF$ of the surface element. \hat{n} is the unit surface normal (Fig. 1). The corresponding spectral distribution functions are given by $E_\lambda = dE / d\lambda$ [Wm^{-3}] and $L_\lambda = dL / d\lambda$ [$Wm^{-3}sr^{-1}$]. \hat{E}_λ and \hat{L}_λ denote relative spectral distribution functions (spectral distribution functions in an arbitrary unit) (Judd, 1975). From the above definitions:

$$dE = L \cos\theta d\omega = L \hat{n} \cdot \hat{l} d\omega. \quad (1)$$

3.2 The Atmospheric Model

Due to the scattering and absorption of light within the atmosphere, an object which moves away from the observer changes its color depending on the distance from the observer, the current weather conditions and the pollution of the air. The atmospheric effect is simulated by the atmospheric model (Schachter, 1983):

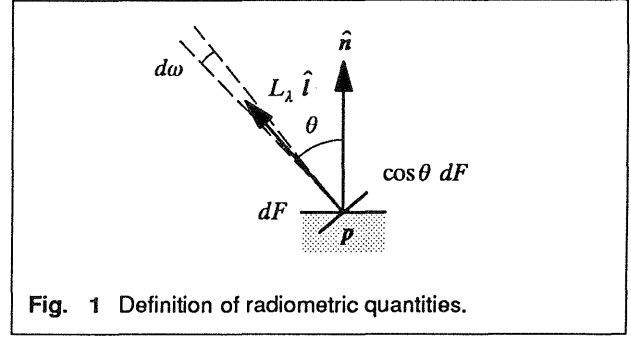
$$L_\lambda = L_{0\lambda} \tau_{a\lambda}^{d/d_a} + L_{\infty\lambda} (1 - \tau_{a\lambda}^{d/d_a}). \quad (2)$$

$L_{0\lambda}$ represents the **true object color**. This is the light which leaves the surface of an object towards the observer. L_λ represents the **apparent object color**. This is the light which reaches the observer at a distance d from the object. $L_{\infty\lambda}$ represents the **horizon color** which is L_λ for $d \rightarrow \infty$. $\tau_{a\lambda}$ is the spectral transmittance of the atmosphere. This is the fraction of light energy which is neither absorbed nor scattered away from the straight direction of light propagation within the reference distance d_a . The atmosphere described by (2) is homogeneous and isotropic. Note that the term **color** is used for simplicity though $L_{0\lambda}$, L_λ and $L_{\infty\lambda}$ are **color stimuli** in terms of spectral radiance.

3.3 The Light Source Model

Natural daylight is assumed to be composed of direct sunlight, diffuse ambient light and diffuse skylight.

The direct **sunlight** (Fig. 2) is defined by the direction \hat{d}_s to the light source (the sun) and by the solid angle $\Omega_s \ll 2\pi$ and the radiance $L_{s\lambda} = k_s \hat{L}_\lambda$ of the incident light. k_s is a weighting factor. By (1), the irradiance $E_{s\lambda}$ of the sunlight incident at a point p on a surface F is



$$E_{s\lambda} = \int_0^{\Omega_s} L_{s\lambda} \hat{n} \cdot \hat{l} d\omega \approx k_s \hat{L}_\lambda \hat{n} \cdot \hat{d}_s \Omega_s. \quad (3)$$

The diffuse **ambient light** (Fig. 2) is a uniform illumination term. It is defined by the radiance $L_\lambda = k_u \hat{L}_\lambda$ of the incident light. k_u is a weighting factor. By (1), the irradiance $E_{u\lambda}$ of the ambient light incident at a point p on a surface F is

$$E_{u\lambda} = \int_0^{2\pi} L_{u\lambda} \hat{n} \cdot \hat{l} d\omega = k_u \hat{L}_\lambda \pi. \quad (4)$$

The diffuse **skylight** (Fig. 3) is sunlight scattered by the atmosphere. It is emitted by the sky hemisphere above the horizon. Because of its large radius, all objects are approximately in the center of the sky hemisphere. The skylight is defined by the direction \hat{d}_h to the zenith which is the highest point of the sky hemisphere, the parameter $m_h > 0$ (see below) and the radiance $L_\lambda = k_h \hat{L}_\lambda$ of the incident light. k_h is a weighting factor. By (1), the irradiance $E_{h\lambda}$ of the skylight incident at a point p on a surface F is

$$E_{h\lambda} = \int_0^{\Omega} L_{h\lambda} \hat{n} \cdot \hat{l} d\omega \approx k_h \hat{L}_\lambda \sum_{i=1}^{4m_h^2} \delta_i \hat{n} \cdot \hat{l}_i \Delta\omega. \quad (5)$$

$\Omega \leq 2\pi$ represents the part of the sky hemisphere with $\hat{n} \cdot \hat{l} > 0$ and $\hat{d}_s \cdot \hat{l} > 0$ which is visible from p . The solid angle 2π is subdivided into $4m_h^2$ sky facets (m_h facets in polar direction \times $4m_h$ facets in azimuth direction) of equal size $\Delta\omega = 2\pi/(4m_h^2)$ and the integral is approximated by a sum. \hat{l}_i is the direction to the center of the i -th sky facet. The summation is done for all facets the centers of which are visible from p . $\delta_i = 1$ if the center of the i -th sky facet is visible from p , and $\delta_i = 0$ else.

The **illumination geometry** is defined by \hat{d}_s , Ω_s , \hat{d}_h and m_h .

Kaneda et al. (Kaneda, 1991) model natural daylight as being composed of direct sunlight and diffuse, non-uniformly incident skylight. The contribution of the skylight is determined by integrating over the visible parts of the sky dome which is subdivided into band sources. Wavelength dependency as well as absorption and scattering in a non-homogeneous atmosphere are taken into account. The discretization of distributed light sources is described by Verbeck & Greenberg (Verbeck, 1984).

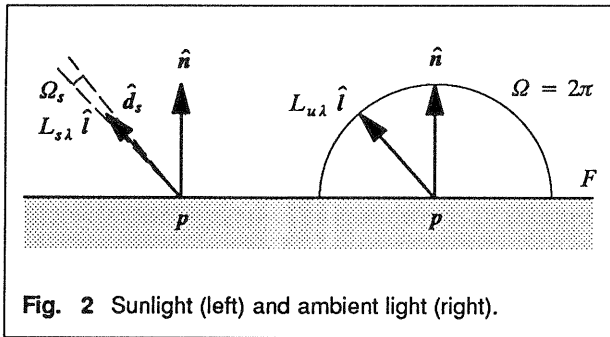


Fig. 2 Sunlight (left) and ambient light (right).

3.4 The Material Model and the Illumination Model

The illumination model expresses the radiance L_λ of the light which leaves a point on the interface between two materials in a given direction. L_λ depends on the roughness of the material interface and the illumination and the materials on both sides of the material interface. The full illumination model (a slight modification of the model by Hall & Greenberg (Hall, 1983) is used) will not be given in detail here. Instead, for an opaque, diffusely reflecting surface illuminated by natural daylight (section 3.3), the radiance L_λ of the reflected light is uniformly distributed in all directions and the illumination model reduces to

$$L_\lambda = k_d \rho_{d\lambda} (E_{s\lambda} + E_{u\lambda} + E_{h\lambda}). \quad (6)$$

k_d is the weight of the diffusely reflected component and $\rho_{d\lambda}$ [sr^{-1}] is the diffuse reflectance (directional hemispherical reflectance) of the material. $E_{s\lambda}$, $E_{u\lambda}$ and $E_{h\lambda}$ are the irradiances due to the incident sunlight, ambient light and skylight according to (3), (4) and (5).

3.5 The Camera Model

World coordinates define locations in three-dimensional object space, **image coordinates** define locations in the two-dimensional image plane of a camera and **bitmap coordinates** define locations in the two-dimensional pixel raster of a digital image.

The camera model represents a calibrated camera in three-dimensional object space. The **interior orientation** of the camera consists of the calibrated focal length, the image coordinates of a number of fiducial marks and the center and amount of the radial image distortion due to the non-ideal optics of the camera. The fiducial marks are not affected by the radial image distortion. Therefore, they define the image coordinate system in the image plane and allow to derive a linear mapping between the homogeneous image coordinates and the homogeneous bitmap coordinates of a digitized image. The **exterior orientation** of the camera consists of the three world coordinates of the camera position and the three angles of the camera orientation in object space.

3.6 The Geometrical Object Model

A geometrical object is either a planar convex or concave polygon, a polyhedron or a sphere. Each geometrical object has a **material attribute** which is a reference into the materi-

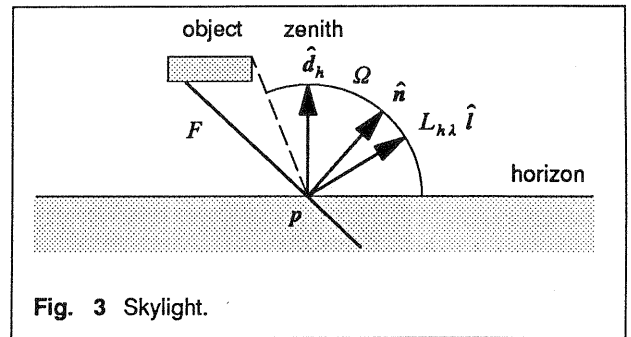


Fig. 3 Skylight.

al library (Fig. 4).

4. INFORMATION FROM DIGITAL COLOR IMAGES

The aim of this work is to produce realistic computer-generated color images which aid to the judgement of aesthetic properties of planned buildings. These **artificial objects** are embedded into the existing environment by photomontage. The **natural environment** is represented by a number of digital site photographs. During an interactive preprocessing step which is supported by the program **PREPARE** (Fig. 4), a three-dimensional description of the natural environment is created by retrieving geometrical and non-geometrical information from the site photographs.

The models (section 3) are formulated in terms of the wavelength. Consequently, RGB triplets retrieved from input images have first to be converted to equivalent spectral distribution functions. A simple and efficient conversion method is detailed in appendix A.

In this section, a number of inversions are formulated. The term **inversion** stands for solving an equation or a system of equations given by one of the models (section 3) for one or more unknown model parameters.

4.1 Inversion of the Camera Model

Each of the digital color images which represent the natural environment is geometrically corrected to eliminate the effect of the radial image distortion. The geometrically corrected images are called the **input images** (Fig. 4).

For each input image, the six unknowns of the exterior orientation are determined separately from the known world coordinates and the manually identified image coordinates of at least three control points. More control points help to refine the result. This is the resection in space or **first inversion of the camera model**. Each control point adds two equations to a system of non-linear equations which is iteratively solved, starting from a user-specified estimation of the solution. The result of the resection in space is converted to a 4x4 matrix which expresses the linear mapping from homogeneous world coordinates to homogeneous image coordinates. Since this mapping will be performed very often during rendering (section 6), its linearity is important for efficiency. The non-linearity introduced by the radial image distortion was previously eliminated by the geometrical correction.

The geometry of relevant parts of the natural environment is

approximated by planar polygons in object space. These define the **scene geometry**. Relevant parts of the natural environment are those interacting with the planned building with respect to hiding, shadowing and interreflection.

The world coordinates of a polygon vertex are determined from its manually identified image coordinates in two or more input images with different exterior orientation. This is the intersection in space or the **second inversion of the camera model**. The geometrical properties of a polygon are defined by its coplanar vertices, while the non-geometrical properties of a polygon are given by an **image attribute** and a **material attribute**. The image attribute references one of the input images. The material attribute is a reference into the material library (Fig. 4). The referenced material description defines all material properties except for the diffuse reflectance $\rho_{d\lambda}$ which is retrieved at rendering time from one of the input images (sections 4.3 and 6). The default input image for retrieving $\rho_{d\lambda}$ is indicated by the image attribute.

The illumination geometry (section 3.3) is determined as follows: The solid angle Ω_s of incident sunlight is calculated from the distance to the sun and the radius of the sun. The direction \hat{d}_s to the sun is determined by a point on an object and the corresponding point on the object's shadow by intersection in space. The direction \hat{d}_h to the zenith is determined similarly, e.g. by two points on the same vertical edge of a house. Since the world coordinate system may be selected arbitrarily, the zenith direction is not known a priori. $m_h > 0$ is set arbitrarily.

Details about resection and intersection in space are not detailed here. These are basic procedures in photogrammetry (Wolf, 1983) (Rüger, 1987).

4.2 Inversion of the Atmospheric Model

The **first inversion of the atmospheric model** involves solving the equation of the atmospheric model (2) for the spectral transmittance $\tau_{a\lambda}$ of the atmosphere.

Given are the horizon color $L_{\infty\lambda}$ and the reference distance $d_a = 1$. $L_{\infty\lambda}$ is derived from a suitable RGB triplet which is manually selected in one of the input images (appendix A). p_i ($i = 1 \dots n$, $n \geq 2$) are known locations in object space. They are situated on the surfaces of objects of the same opaque, diffusely reflecting material. The p_i are manually identified on previously determined polygons in object space (section 4.1). The known apparent object color $L_{i\lambda}$ is the radiance of the light reaching the camera associated with one of the input images at the known distance d_i from p_i . $L_{i\lambda}$ is derived from the RGB triplet of the reconstructed image function at p_i' (appendix A). p_i' are the image coordinates of p_i in the selected input image.

By inserting into (2), each sample contributes one equation

$$L_{0\lambda} \tau_{a\lambda}^{d_i} + L_{\infty\lambda} (1 - \tau_{a\lambda}^{d_i}) - L_{i\lambda} = 0 \quad (7)$$

to a system of n non-linear equations which is redundant for $n > 2$. For each wavelength within the visible spectrum, the

system of equations (7) is iteratively solved for the unknowns which are the true object color $L_{0\lambda}$ and the spectral transmittance $\tau_{a\lambda}$ of the atmosphere. $L_{0\lambda}$ is of no interest since it expresses no general property of the scene. The iteration is started with $\tau_{a\lambda} = 1$ and $L_{0\lambda} = L_{j\lambda}$, such that $d_j = \min(d_i)$.

A simplifying assumption is that the radiance $L_{0\lambda}$ of the light leaving the objects towards the observer is the same at all locations p_i . The radiance of the diffusely reflected light is uniformly distributed in all directions but it depends on the illumination of the surface and the orientation of the surface relative to the light sources.

Nakamae et al. (Nakamae, 1986) use an equivalent method based on the same atmospheric model (2). Wavelength dependency is not considered and world coordinates are obtained from topographical maps.

The **second inversion of the atmospheric model** involves solving the equation of the atmospheric model (2) for the true color $L_{0\lambda}$ of an object. This inversion will also be used during rendering (section 6).

Given are the horizon color $L_{\infty\lambda}$, the spectral transmittance $\tau_{a\lambda}$ of the atmosphere and the reference distance $d_a = 1$. $L_{\infty\lambda}$ and $\tau_{a\lambda}$ are known from the first inversion of the atmospheric model (see above). p is a known location in object space. The known apparent object color L_λ is the radiance of the light reaching the camera associated with one of the input images at the known distance d from p . L_λ is derived from the RGB triplet of the reconstructed image function at p' (appendix A). p' are the image coordinates of p in the selected input image.

Inserting into (2) and solving for $L_{0\lambda}$ yields

$$L_{0\lambda} = (L_\lambda - L_{\infty\lambda}) \tau_{a\lambda}^{-d} + L_{\infty\lambda} \quad (8)$$

4.3 Inversion of the Illumination Model

The **first inversion of the illumination model** involves solving the equation of the illumination model (6) for the weights k_s , k_u and k_h of the three illumination components which make up natural daylight (section 3.3).

Given are the scene geometry (section 4.1) and the illumination geometry \hat{d}_s , Ω_s , \hat{d}_h and m_h (sections 3.3 and 4.1). \hat{L}_λ is the known relative spectral distribution function of the daylight components. p_i ($i = 1 \dots n$, $n \geq 3$) are known locations in object space. They are situated on the surfaces of objects of the same opaque, diffusely reflecting material with material parameters $k_d = 1$ and $\rho_{d\lambda}$, where $\rho_{d\lambda}$ is known up to a constant factor only. Each p_i receives a different amount of illumination by the natural daylight. The p_i are manually identified on previously determined polygons in object space (section 4.1). The known apparent object color $L_{i\lambda}$ is the radiance of the light reaching the camera associated with one of the input images at the known distance d_i from p_i . $L_{i\lambda}$ is derived from the RGB triplet of the reconstructed image function at p_i' (appendix A). p_i' are the image coordinates of p_i in the selected input image. The true object color $L_{0i\lambda}$ is determined from $L_{i\lambda}$ by the second inversion of the atmospheric

ic model (the effect of the atmosphere is eliminated) (section 4.2).

By inserting into (6), each sample contributes one equation

$$L_{0i\lambda} = \rho_{d\lambda} (E_{si\lambda} + E_{ui\lambda} + E_{hi\lambda}) \quad (9)$$

to a system of n linear equations which is redundant for $n > 3$. $E_{si\lambda}$, $E_{ui\lambda}$ and $E_{hi\lambda}$ are the irradiances due to the incident sunlight, ambient light and skylight. Since the scene geometry and the illumination geometry are known, they can be calculated according to (3), (4) and (5). For each wavelength within the visible spectrum, the system of equations (9) is solved for the unknowns which are the weights k_s , k_u and k_h of the daylight components. Finally, the weights are averaged within the visible spectrum. Since $\rho_{d\lambda}$ is known up to a constant factor only, k_s , k_u and k_h are the relative weights of the daylight components.

Nakamae et al. (Nakamae, 1986) and Thirion (Thirion, 1992) determine the ratio of illumination by direct sunlight and ambient light. Skylight, wavelength dependency and the effect of the atmosphere are not considered.

The **second inversion of the illumination model** involves solving the equation of the illumination model (6) for the diffuse reflectance $\rho_{d\lambda}$ of a material. This inversion will be used during rendering (section 6).

Given are the scene geometry (section 4.1) and the illumination geometry \hat{d}_s , Ω_s , \hat{d}_h and m_h (sections 3.3 and 4.1). The radiances $k_s \hat{L}_\lambda$, $k_u \hat{L}_\lambda$, $k_h \hat{L}_\lambda$ of the daylight components are known from the first inversion of the illumination model (see above). p is a known location in object space. It is situated on the surface of an object of an opaque, diffusely reflecting material with material parameter $k_d > 0$. The known apparent object color L_λ is the radiance of the light reaching the camera associated with one of the input images at the known distance d from p . L_λ is derived from the RGB triplet of the reconstructed image function at p' (appendix A). p' are the image coordinates of p in the selected input image. The true object color $L_{0\lambda}$ is determined from L_λ by the second inversion of the atmospheric model (the effect of the atmosphere is eliminated) (section 4.2).

Inserting into (6) and solving for $\rho_{d\lambda}$ yields

$$\rho_{d\lambda} = L_{0\lambda} (k_d (E_{s\lambda} + E_{u\lambda} + E_{h\lambda}))^{-1}. \quad (10)$$

$E_{s\lambda}$, $E_{u\lambda}$ and $E_{h\lambda}$ are the irradiances due to the incident sunlight, ambient light and skylight. Since the scene geometry and the illumination geometry are known, they can be calculated according to (3), (4) and (5). Since the relative weights k_s , k_u and k_h were used, also $\rho_{d\lambda}$ is known up to a constant factor only.

Thirion (Thirion, 1992) determines the reflectance of a material without considering skylight, wavelength dependency and the effect of the atmosphere.

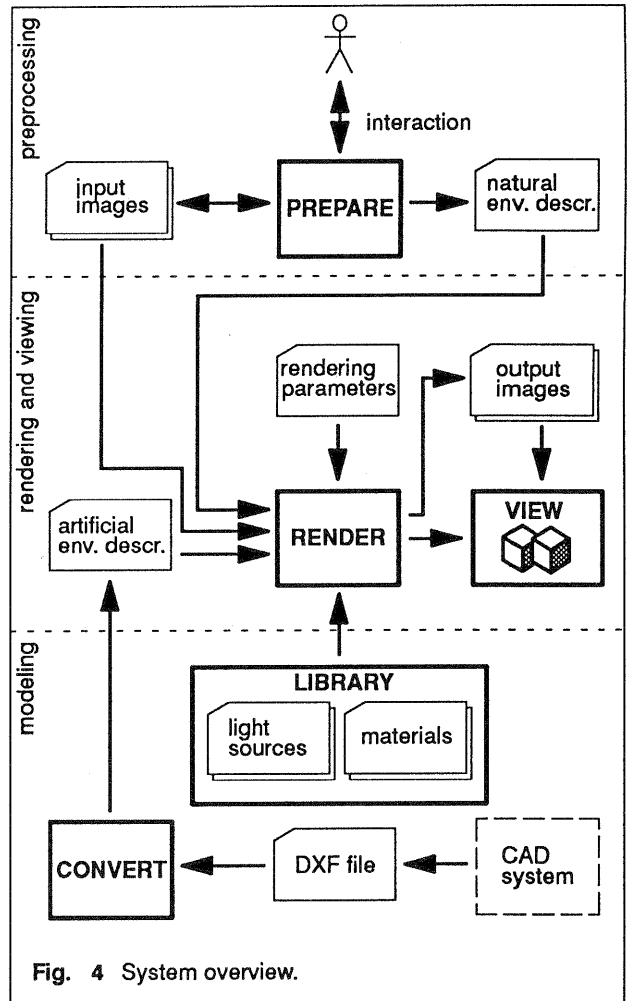


Fig. 4 System overview.

5. ENVIRONMENT DESCRIPTIONS

The **natural environment description** (Fig. 4) contains geometrical and non-geometrical data about the natural environment of the planned building: Atmospheric parameters ($L_{\infty\lambda}$, $\tau_{a\lambda}$, d_a), illumination parameters (\hat{d}_s , Ω_s , k_s , k_u , m_h , \hat{d}_h , k_h , L_λ) and polygons (vertices, material attribute, image attribute). Most of this information is retrieved from the input images during the interactive preprocessing step (section 4). Additionally, the natural environment description contains the interior and exterior orientation and the file name of each of the input images.

The **artificial environment description** (Fig. 4) contains the CAD model of the planned building with additional artificial light sources, if required. The program **CONVERT** (Fig. 4) converts data from the widely used DXF format (Autodesk, 1988) to the required data format.

6. RENDERING

During the final rendering step (program **RENDER**) (Fig. 4), the input images and the natural and artificial environment description (section 5) are used to generate the **output images**. These show the planned building embedded in the existing environment from the perspectives of the input images. The rendering algorithm is an extension to conven-

tional ray-tracing. Ray-tracing was introduced by Whitted (Whitted, 1980). It is assumed that the reader is familiar with the principle of recursive ray-tracing in object space.

6.1 Setup

One of the input images is selected as the **current input image**. The **current camera** is the camera associated with the current input image. It represents the observer in object space and remains unchanged during the generation of the current output image.

6.2 Independent Pixel Processing

A **natural object** or **natural light source** is part of the natural environment description (section 5). Each facet of the discretized sky hemisphere (section 3.3) is treated as an individual natural light source. An **artificial object** or **artificial light source** is part of the artificial environment description (section 5). A **primary ray** originates at the center of projection of the current camera. A **secondary ray** is generated after reflection or refraction at a material interface.

Several cases are identified:

Case A. A primary ray does not hit any object: The intersection point p of the ray and the image plane of the current camera is mapped from world coordinates to image coordinates p' of the current input image. The RGB triplet of the reconstructed image function at p' is converted to a spectral distribution function L_λ (appendix A) and returned.

Case B. A secondary ray does not hit any object: The horizon color $L_{\infty\lambda}$ (sections 3.2 and 4.2) is returned if the ray direction is above the horizon.

Case C. Any ray hits an artificial object: The illumination model (6) is evaluated at the intersection point p of the ray and the artificial object under consideration of the illuminating natural and artificial light sources. Subsequently, the atmospheric model (2) is evaluated based on the known distance d along the ray and the result L_λ is returned. Depending on the object material, a reflected and / or a refracted ray may be recursively traced. All material properties come from the member of the material library (Fig. 4) which is referenced through the object's material attribute.

Case D. Any ray hits a natural object: The intersection point p of the ray and the natural object is mapped from world coordinates to image coordinates p' of one of the input images. This is the current input image if the ray is a primary ray; otherwise it is the input image referenced through the polygon's image attribute (section 4.1). The RGB triplet of the reconstructed image function at p' is converted to a spectral distribution function L_λ (appendix A) which represents the apparent color of the natural object. The true color $L_{0\lambda}$ of the natural object is determined by the second inversion of the atmospheric model (section 4.2) based on the known distance d_0 between p and the camera associated with the selected input image (the effect of the atmosphere is eliminated). The diffuse reflectance $\rho_{d\lambda}$ of the object material

is determined from $L_{0\lambda}$ by the second inversion of the illumination model (section 4.3). All other material properties, including k_d , come from the member of the material library (Fig. 4) which is referenced through the polygon's material attribute.

Three subcases of case D are identified:

Case D1. The natural object is illuminated by an artificial light source: The illumination model (6) is evaluated at p under consideration of the illuminating artificial light source and the result is added to the true object color $L_{0\lambda}$. Subsequently, the atmospheric model (2) is evaluated based on the known distance d along the ray and the result L_λ is returned.

Case D2. The natural object is illuminated by a natural light source: The illumination model is not evaluated since the illumination effect at p is already represented by the true object color $L_{0\lambda}$. The atmospheric model (2) is evaluated based on the known distance d along the ray and the result L_λ is returned.

Case D3. The natural object is not illuminated by a natural light source due to an artificial object only. The irradiance E_λ due to the natural light source is calculated at p as if there were no artificial objects in the scene. The illumination model (6) is evaluated at p with a **negative** irradiance $-E_\lambda$ and the result is added to the true object color $L_{0\lambda}$. Subsequently, the atmospheric model (2) is evaluated based on the known distance d along the ray and the result L_λ is returned.

Depending on the object material, a reflected and / or a refracted ray may be recursively traced for each of the three subcases D1 - D3.

6.3 Change of Perspective

Restarting at the setup step (section 6.1) with another current input image and the corresponding current camera allows to generate a different view of the scene without any changes in the natural or artificial environment description.

6.4 Output and Viewing

The program **VIEW** (Fig. 4) displays the finished part of an image the computation of which is still in progress. This allows to interrupt the calculation of not very promising images. **VIEW** may run on a local workstation while **RENDER** runs concurrently on a remote host. Image data is transmitted in ASCII format through a UNIX pipe.

7. EXAMPLES

Three examples will be presented in this section. Additional information about the examples is given in Tab. 1.

Example 1. Gallery: This is the test scene on the campus of ETH-Hoenggerberg, Zurich. Fig. 5, top left and bottom left, shows the natural environment on a sunny day. The gallery (supports, roof, floor), the horizontal lawn plane and the main buildings in the background were approximated by planar polygons during preprocessing (section 4.1). The horizon

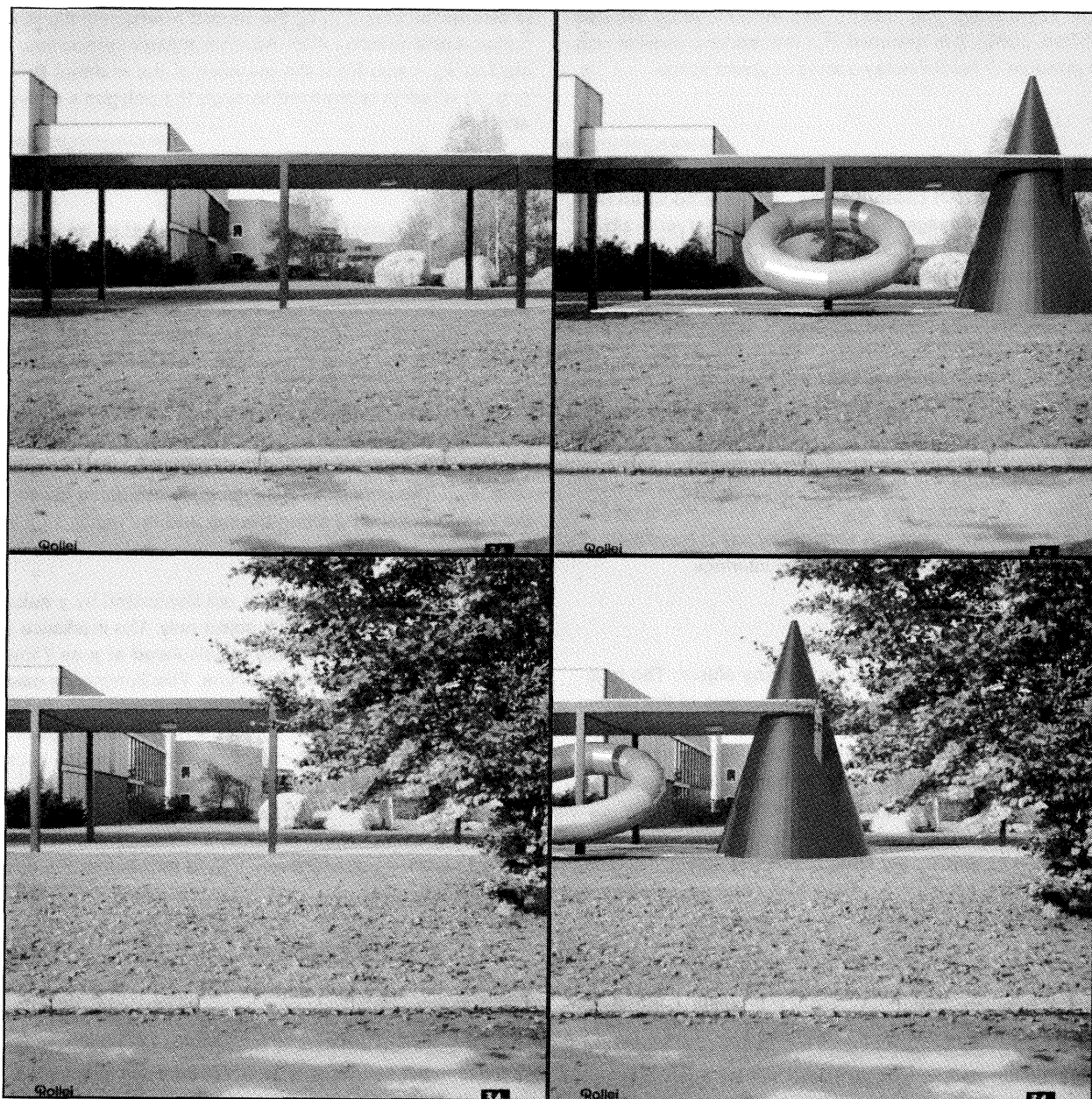


Fig. 5 Example 1. Gallery.

color $L_{\infty\lambda}$ was set equal to the sky color. Samples on the lawn plane were used to determine the spectral transmittance $\tau_{a\lambda}$ of the atmosphere by the first inversion of the atmospheric model (section 4.2). Samples of various incident illumination were selected on the concrete walls of the background building on the left and used to determine the relative weights k_s, k_u, k_h of the daylight components by the first inversion of the illumination model (section 4.3). Fig. 5, top right and bottom right, shows some primitive solids embedded in the natural environment. Note the shadow of the natural support cast onto the artificial torus, the geometrically correct interpenetration of the cone with the gallery and the shadow of the torus cast onto the ground. Both perspectives were rendered with no change in the natural or artificial environment description, simply by selecting different current input images with the corresponding current cameras.

Example 2. Bridge: The example shows the planned wood-

en bridge at Bueren an der Aare, Kanton Bern, which is intended to replace the historical bridge recently destroyed by a fire. Fig. 6, top left, shows the natural environment on a sunny day. The house on the left (wall, balconies, roof) and the horizontal water plane were approximated by planar polygons during preprocessing (section 4.1). The horizon color $L_{\infty\lambda}$ was set equal to the sky color. Samples on the water plane were used to determine the spectral transmittance $\tau_{a\lambda}$ of the atmosphere by the first inversion of the atmospheric model (section 4.2). Samples of various incident illumination were selected on the house and used to determine the relative weights k_s, k_u, k_h of the daylight components by the first inversion of the illumination model (section 4.3). The supports will be used for the new bridge. Fig 6, top right, bottom left and bottom right, shows the new bridge from two different perspectives. Note the shadow and the specular reflection on the water surface. In Fig. 6, top right and bottom right, the unnatural regularity of the reflection is destroyed by a sto-

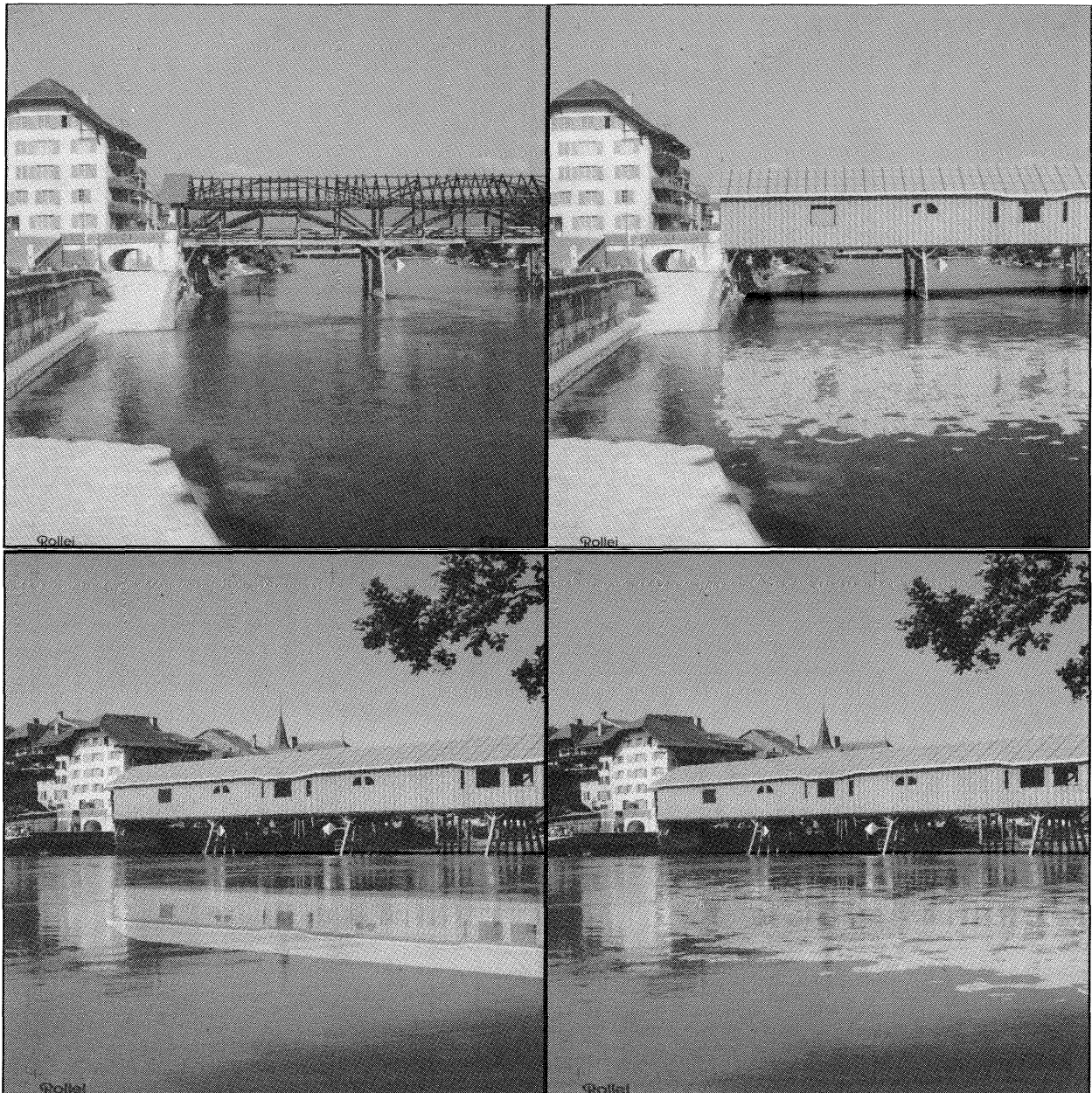


Fig. 6 Example 2. Bridge.

chastic perturbation added to the local normal vector of the water surface. The perturbation was generated based on the method of Haruyama & Barsky (Haruyama, 1984) which was extended to three dimensions and used as a solid texture. Blinn (Blinn, 1978) introduced surface normal perturbation. Solid textures were introduced by Peachey (Peachey, 1985) and Perlin (Perlin, 1985).

Example 3. Courtyard: The example shows a project for the redesign of a courtyard in the city of Zurich. Fig. 7, top left, shows the natural environment on a winter day with overcast sky. The illumination is completely diffuse and consists of ambient light and skylight only. Parts of the houses and the horizontal ground plane were approximated by planar polygons during preprocessing (section 4.1). The atmospheric effect has not been taken into account. Samples of various incident illumination were selected on the white house in the corner and used to determine the relative weights k_s , k_u , k_h

of the daylight components by the first inversion of the illumination model (section 4.3). Fig 7, top right, bottom left and bottom right, shows the planned building from various perspectives. Note the specular reflection of natural and artificial objects in the windows. There is a diffuse shadow below the arcades. The somewhat noisy appearance is mainly due to a coarse discretization of the sky hemisphere by 4 sky facets.

All example images were rendered with a resolution of 512 x 512 pixels using an antialiasing strategy based on adaptive stochastic sampling (Cook, 1984) (Cook, 1986). Based on the statistical variance of the returned color values, 4, 8, 12 or 16 rays per pixel were used, resulting in an average per image of between 4.0 and 4.5 rays per pixel. The relative spectral distribution function $\hat{L}_{65\lambda}$ of the CIE standard illuminant D_{65} (Judd, 1975) was used for the relative spectral distribution function \hat{L}_λ of the three daylight components. For the calculation of the relative weights k_s , k_u , k_h of the day-

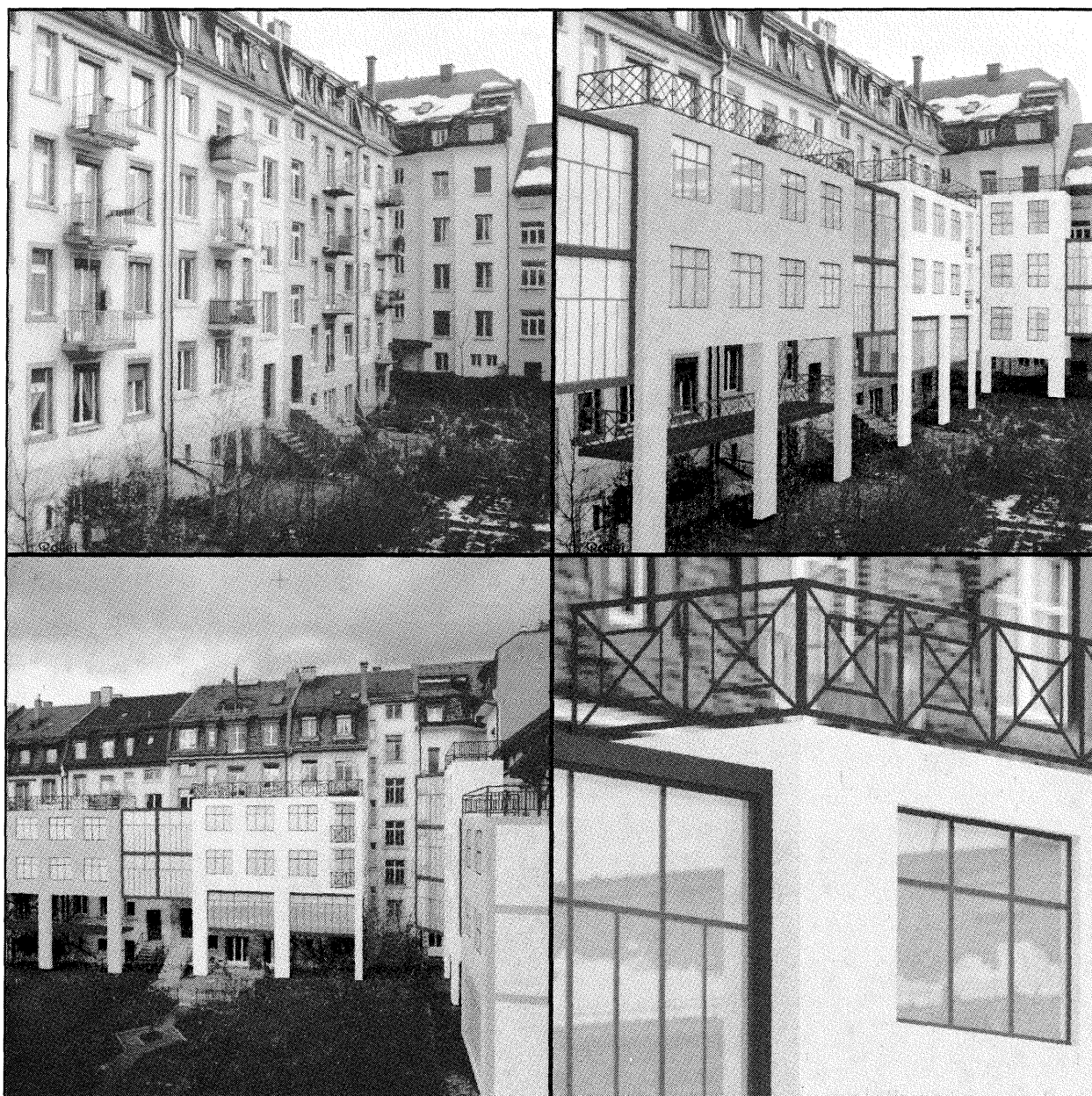


Fig. 7 Example 3. Courtyard.

light components by the first inversion of the illumination model (section 4.3) $Q_{d\lambda} \equiv 1$ was assumed for the material at all sample points. This seems to be a reasonable choice since the material was always gray or white and $Q_{d\lambda}$ has to be known up to a constant factor only. Subsequently, k_s , k_u and k_h were used as calculated. For the simulation, spectral curves were reduced to a total of 9 spectral samples within the visible spectrum. After the simulation, spectral distribution functions were reconstructed from the spectral samples and converted to the RGB color space of a specific output device (Hall, 1989). Image rendering was performed on a CONVEX-C2 computer with a poorly vectorizing code.

8. SUMMARY

The paper presents a method to produce realistic computer-generated color images which aids to the judgement of aesthetic properties of planned buildings. The planned buildings

are embedded into the existing environment by photomontage. During an interactive preprocessing step, a three-dimensional description of the existing environment is retrieved from the site photographs (input images). In a second step, the input images, the information retrieved from the input images (the natural environment description) and the CAD model of the planned building (the artificial environment description) are used to generate the final images. These show the artificial object (the planned building) embedded in the existing environment from the perspectives of the input images.

Consistency with the models is maintained during preprocessing (section 4) and rendering (section 6). The models (section 3) are formulated in terms of the wavelength. Therefore, RGB triplets retrieved from input images are converted to equivalent spectral distribution functions (appendix A).

Extensions to previous methods have been presented for retrieving atmospheric-, illumination- and material parameters from the input images (section 4). A drawback is the limited complexity of the scene geometry which can be handled by the interactive preprocessor. However, the preprocessing step has to be done only once for a given scene. Once the preprocessing step is completed, case studies can be investigated flexibly by simply changing the artificial environment description and rendering a series of new images.

Conventional ray-tracing is strictly additive, whereas the presented approach extends ray-tracing to an additive and subtractive process: sometimes illumination has to be added, sometimes it has to be removed. The extension is straightforward and implied by the nature of the problem for which it was designed. No changes in the illumination model (6) are required. The key is to pass a negative irradiance to the illumination model in case D3.

The presented approach allows to add an arbitrary number of artificial objects and artificial light sources to an existing scene. The rendering algorithm is based on ray-tracing which works entirely in three-dimensional object space and handles the interaction between the artificial object and the existing environment with respect to hiding, shadowing and interreflection.

The system consists of the programs PREPARE, CONVERT, RENDER and VIEW (Fig. 4). Rendering parameters allow to trade off speed versus image quality. At an early stage of the design process, quick looks can be generated, e.g. at a low resolution or by using simpler models. Tabulated physical data is used directly in an extendable library. This frees the user from inventing some fundamental material and light source properties, though some of the coefficients still have to be selected empirically.

The examples show some of the subtle effects which make up the overall appearance of a building: the three-dimensional shapes and their proportions, the surface textures and colors which are determined by the selected materials, the proportions between light and shadow, the integration of the object into its environment and the effects which are determined by daytime, season, current weather conditions and by the selection of the observer position with respect to foreground and background (Leonhardt, 1984).

9. ACKNOWLEDGEMENTS

I would like to thank Prof. Dr. A. Gruen and Z. Parsic, Institute of Geodesy and Photogrammetry at the ETH Zurich, who enabled me to use the institute's photographic equipment, Dr. U. Walder for the construction plans of the bridge in example 2 (project by Walder & Marchand AG, Guemligen, Moor & Hauser AG, Bern) and Dr. G. Scheibler, the architect of the courtyard project in example 3 (project by Architekturwerkstatt Ruetschistrasse, Zurich). Special thanks to Z. Despot for the measurement of control points and to L. Hurni and H. Stoll, Institute of Cartography at the ETH Zurich, for the reproduction of the images.

Tab. 1 Example data.			
	example 1	example 2	example 3
input images	3	8	9
nat. polygons	38	16	17
Ω_s [sr]	0 . 0004	0 . 0004	—
k_s	4111 . 65	4639 . 82	—
k_u	0 . 14	0 . 13	0 . 53
m_h	2	2	1
k_h	0 . 72	0 . 51	0 . 65
CPU [min]	201 .. 239	225 .. 292	153 .. 221

10. REFERENCES

- Autodesk Inc., 1988. AutoCAD10 Reference Manual. Appendix C: Drawing Interchange and File Formats.
- BD&C, 1990. Computer Graphics Facilitate Approvals. Building Design & Construction, 31 (7) : 16.
- Blinn, J. F., 1978. Simulation of Wrinkled Surfaces. Proceedings SIGGRAPH '78. Computer Graphics, 12 (3): 286-292.
- Cook, R. L., T. Porter and L. Carpenter, 1984. Distributed Ray Tracing. Proceedings SIGGRAPH '84. Computer Graphics, 18 (3) : 137-145.
- Cook, R. L., 1986. Stochastic Sampling in Computer Graphics. ACM Transactions on Graphics, 5 (1): 51-72.
- Doi, A., M. Aono, N. Urano and K. Sugimoto, 1991. Data visualization using a general-purpose renderer. IBM Journal of Research and Development, 35 (1/2) : 45-58.
- Durisch, P. 1992. Ein Programm für die Visualisierung projektierter Bauwerke mittels Fotomontage. Ph.D. Dissertation No. 9599 ETH Zurich. vdf, Zurich.
- Feibush, E. A., M. Levoy and R. L. Cook, 1980. Synthetic Texturing Using Digital Filters. Proceedings SIGGRAPH '80. Computer Graphics, 14 (3) : 294-301.
- Glassner, A. S., 1989. How to Derive a Spectrum from an RGB Triplet. IEEE Computer Graphics & Applications, 9 (4) : 95-99.
- Hall, R. A. and D. P. Greenberg, 1983. A Testbed for Realistic Image Synthesis. IEEE Computer Graphics & Applications, 3 (8) : 10-20.
- Hall, R. A., 1989. Illumination and Color in Computer Generated Imagery. Springer, New York.
- Haruyama, S. and B. A. Barsky, 1984. Using Stochastic Modeling for Texture Generation. IEEE Computer Graphics & Applications, 4 (3) : 7-19.
- Judd, D. B. and G. Wyszecki, 1975. Color in Business, Science and Industry. Third Edition. John Wiley & Sons, New York.
- Kaneda, K., F. Kato, E. Nakamae, T. Nishita, H. Tanaka and T. Noguchi, 1989. Three Dimensional Terrain Modeling and Display for Environmental Assessment. Proceedings SIGGRAPH '89. Computer Graphics, 23 (3) : 207-214.
- Kaneda, K., T. Okamoto, E. Nakamae and T. Nishita, 1991. Photorealistic images synthesis for outdoor scenery under various atmospheric conditions. The Visual Computer, 7 : 247-258.

Leonhardt, F., 1984. *Brücken. Ästhetik und Gestaltung*. 2. Auflage. Deutsche Verlags-Anstalt, Stuttgart.

Maver, T.W., C. Purdie and D. Stearn, 1985. *Visual Impact Analysis - Modelling and Viewing the Natural and Built Environment*. *Computers & Graphics*, 9 (2) : 117-124.

Nakamae, E., K. Harada, T. Ishizaki and T. Nishita, 1986. *A Montage Method: The Overlaying of the Computer Generated Images onto a Background Photograph*. *Proceedings SIGGRAPH '86*. *Computer Graphics*, 20 (4) : 207-214.

Nakamae, E., T. Ishizaki, T. Nishita and S. Takita, 1989. *Compositing 3D Images with Antialiasing and Various Shading Effects*. *IEEE Computer Graphics & Applications*, 9 (2) : 21-29.

Peachey, D. R., 1985. *Solid Texturing of Complex Surfaces*. *Proceedings SIGGRAPH '85*. *Computer Graphics*, 19 (3) : 279-286.

Perlin, K., 1985. *An Image Synthesizer*. *Proceedings SIGGRAPH '85*. *Computer Graphics*, 19 (3) : 287-296.

Rüger, W., J. Pietschner and K. Regensburger, 1987. *Photogrammetrie*. 5. Auflage. VEB Verlag für Bauwesen, Berlin.

Schachter, B. J., 1983. *Computer Image Generation*. John Wiley & Sons, New York.

Takagi, A., H. Takaoka, T. Oshima and Y. Ogata, 1990. *Accurate Rendering Technique Based on Colorimetric Conception*. *Proceedings SIGGRAPH '90*. *Computer Graphics*, 24 (4) : 263-272.

Terzopoulos, D. and A. Witkin, 1988. *Physically Based Models with Rigid and Deformable Components*. *IEEE Computer Graphics & Applications*, 8 (6) : 41-51.

Thirion, J.-P., 1992. *Realistic 3D Simulation of Shapes and Shadows for Image Processing*. *CVGIP: Graphical Models and Image Processing*, 54 (1) : 82-90.

Uno, S. and H. Matsuka, 1979. *A General Purpose Graphic System for Computer Aided Design*. *Proceedings SIGGRAPH '79*. *Computer Graphics*, 13 (2) : 25-32.

Verbeck, C. P. and D. P. Greenberg, 1984. *A Comprehensive Light Source Description for Computer Graphics*. *IEEE Computer Graphics & Applications*, 4 (7) : 66-75.

Whitted, T., 1980. *An Improved Illumination Model for Shaded Display*. *Communications of the ACM*, 23 (6) : 343-349.

Wolf, P. R., 1983. *Elements of Photogrammetry*. Second Edition. McGraw-Hill, New York.

Wyszecki, G. and W. S. Stiles, 1982. *Color Science: Concepts and Methods, Quantitative Data and Formulas*. Second Edition. John Wiley & Sons, New York.

A. SPECTRAL DISTRIBUTIONS FROM RGB TRIPLETS

The perception of color is determined by the spectral distribution function of the electromagnetic energy entering the eye and by the properties of the human visual system. The color sensation produced by a given color stimulus L_λ can be quantified by a triplet of numbers X, Y, Z :

$$X = k \int_{380}^{780} L_\lambda \bar{x}_\lambda d\lambda; Y = k \int_{380}^{780} L_\lambda \bar{y}_\lambda d\lambda; Z = k \int_{380}^{780} L_\lambda \bar{z}_\lambda d\lambda \quad (11)$$

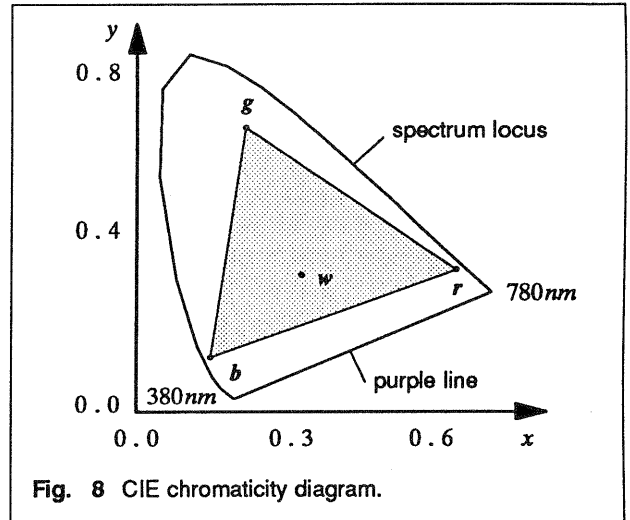


Fig. 8 CIE chromaticity diagram.

$X, Y, Z \geq 0$ are the tristimulus values in the CIE 1931 standard colorimetric system (Judd, 1975) (Wyszecki, 1982). L_λ is the color stimulus in terms of spectral radiance. The CIE color-matching functions $\bar{x}_\lambda, \bar{y}_\lambda, \bar{z}_\lambda$ represent the CIE standard colorimetric observer. k is a normalizing factor.

The chromaticity $f = [x \ y \ z]^T$ of a color is given by

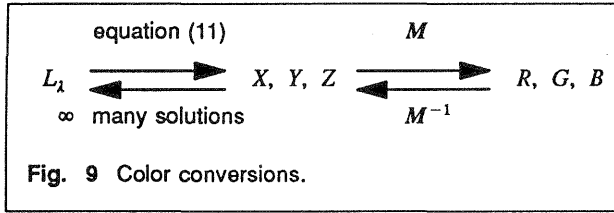
$$x = \frac{X}{X+Y+Z} \quad y = \frac{Y}{X+Y+Z} \quad z = \frac{Z}{X+Y+Z} \quad (12)$$

with $x + y + z = 1$. Equation (12) maps the tristimulus values $F = [X \ Y \ Z]^T$ onto the $(X + Y + Z = 1)$ -plane in CIE XYZ color space. The two-dimensional (x, y) -plot is the CIE chromaticity diagram (Fig. 8). The chromaticities of all physically realizable colors are contained within the area bounded by the spectrum locus and the straight purple line. The spectrum locus is given by the chromaticities of the pure spectral colors.

Two color stimuli are metameric with respect to a given observer $\bar{x}_\lambda, \bar{y}_\lambda, \bar{z}_\lambda$ if their respective tristimulus values are the same but their spectral distribution functions are different. By (11), metameric color stimuli are mapped to the same tristimulus values. The inverse problem of finding a color stimulus with given tristimulus values has therefore (infinitely) many metameric solutions (Fig. 9).

The conversion from RGB color space to L_λ is decomposed into a conversion from RGB color space to CIE XYZ color space and a conversion from CIE XYZ color space to L_λ (Fig. 9).

The RGB color space is defined by the chromaticities r, g, b of the RGB primaries and the chromaticity w of the RGB white point. The chromaticities of all colors which are realizable in the given RGB color space are contained within the triangle r, g, b (Fig. 8). The conversion from CIE XYZ color space to RGB color space is given by the 3×3 matrix M which is derived from r, g, b and w (Judd, 1975) (Hall, 1989):



$$\begin{bmatrix} R \\ G \\ B \end{bmatrix} = M \begin{bmatrix} X \\ Y \\ Z \end{bmatrix}, \quad \begin{bmatrix} X \\ Y \\ Z \end{bmatrix} = M^{-1} \begin{bmatrix} R \\ G \\ B \end{bmatrix}. \quad (13)$$

It is assumed that r, g, b and w are known. In the examples (section 7), the definition values of the standard NTSC monitor (Hall, 1989) were used.

The problem of finding color stimuli L_λ for all RGB triplets in the given RGB color space is equivalent to the problem of finding color stimuli L_λ for all tristimulus values F the chromaticities f of which are contained within the triangle r, g, b :

Given are three basis functions $L_{1\lambda}, L_{2\lambda}, L_{3\lambda} \geq 0$ with tristimulus values F_1, F_2, F_3 and chromaticities f_1, f_2, f_3 , such that $F_1 = f_1 = b, F_2 = f_2 = g, F_3 = f_3 = r$. A color stimulus $L_\lambda \geq 0$ with given tristimulus values $F = [X \ Y \ Z]^T$ is expressed as a linear combination

$$L_\lambda = c_1 L_{1\lambda} + c_2 L_{2\lambda} + c_3 L_{3\lambda} \quad (14)$$

of the basis functions with the weights $c_1, c_2, c_3 \geq 0$.

Inserting (14) into (11)

$$\begin{bmatrix} X \\ Y \\ Z \end{bmatrix} = k \begin{bmatrix} \int_{380}^{780} L_{1\lambda} \bar{x}_\lambda d\lambda \dots \int_{380}^{780} L_{3\lambda} \bar{x}_\lambda d\lambda \\ \vdots \\ \int_{380}^{780} L_{1\lambda} \bar{z}_\lambda d\lambda \dots \int_{380}^{780} L_{3\lambda} \bar{z}_\lambda d\lambda \end{bmatrix} \begin{bmatrix} c_1 \\ c_2 \\ c_3 \end{bmatrix} = D \begin{bmatrix} c_1 \\ c_2 \\ c_3 \end{bmatrix}, \quad (15)$$

premultiplying (15) by M

$$\begin{bmatrix} R \\ G \\ B \end{bmatrix} = M \begin{bmatrix} X \\ Y \\ Z \end{bmatrix} = M D \begin{bmatrix} c_1 \\ c_2 \\ c_3 \end{bmatrix} = W \begin{bmatrix} c_1 \\ c_2 \\ c_3 \end{bmatrix} \quad (16)$$

and solving (16) for c_1, c_2, c_3 yields

$$\begin{bmatrix} c_1 \\ c_2 \\ c_3 \end{bmatrix} = W^{-1} \begin{bmatrix} R \\ G \\ B \end{bmatrix}. \quad (17)$$

The problem which remains is how to generate basis functions $L_{i\lambda} \geq 0$ ($i = 1 \dots 3$) with given tristimulus values F_i . A simple method is explained below:

The visible spectrum from $\lambda = 380 \text{ nm}$ to $\lambda = 780 \text{ nm}$ is

subdivided into three domains: $\lambda_1 \dots \lambda_2, \lambda_2 \dots \lambda_3$ and $\lambda_3 \dots \lambda_4$, such that $380 \text{ nm} = \lambda_1 < \lambda_2 < \lambda_3 < \lambda_4 = 780 \text{ nm}$. The basis function $L_{i\lambda}$ ($i = 1 \dots 3$) is expressed as a linear combination

$$L_{i\lambda} = c_{1i} L_{1i\lambda} + c_{2i} L_{2i\lambda} + c_{3i} L_{3i\lambda}. \quad (18)$$

of piecewise constant functions $L_{ki\lambda}$ ($k = 1 \dots 3$) with

$$L_{ki\lambda} = \begin{cases} 1, & \text{if } \lambda_k \leq \lambda < \lambda_{k+1} \\ 0, & \text{else} \end{cases} \quad (19)$$

Inserting (18) into (11), premultiplying by M and solving for c_{1i}, c_{2i}, c_{3i} (see above) yields the basis function $L_{i\lambda}$. For a constant pair λ_2 and λ_3 , some of the weights c_{1i}, c_{2i}, c_{3i} can be negative. This can result in a piecewise negative color stimulus L_λ which is physically not meaningful. Therefore, the weights c_{1i}, c_{2i}, c_{3i} are calculated for each pair λ_2 and λ_3 within the visible spectrum and the best solution is selected:

One or more metameric solutions with $c_{1i}, c_{2i}, c_{3i} \geq 0$ exist: The candidate with $\max(c_{1i}, c_{2i}, c_{3i}) = \min$ is selected for $L_{i\lambda}$. This condition tries to prevent the energy of $L_{i\lambda}$ from being concentrated in a narrow wavelength band. (The linear combination of three line spectra would result in a color stimulus L_λ which is zero almost everywhere.)

No solution $c_{1i}, c_{2i}, c_{3i} \geq 0$ exists (this can happen for chromaticities near the spectrum locus): A different set of candidates are considered for $L_{i\lambda}$. They are piecewise constant with either value 0 or value $s_i \geq 0$ and with exactly two transitions between 0 and s_i , one at λ_2 and the other at λ_3 . $F_i' = [X_i' \ Y_i' \ Z_i']^T$ are the tristimulus values of the candidate. For each candidate, s_i is calculated such that $Y_i' = Y_i$ and the candidate with $\|F_i' - F_i\|_2 = \min$ is selected for $L_{i\lambda}$.

$L_{1\lambda}, L_{2\lambda}, L_{3\lambda}$ and W^{-1} have to be determined only once for a given RGB color space. Subsequently, finding a color stimulus L_λ with given RGB color values consists of calculating c_1, c_2, c_3 by (17) and linearly combining $L_{1\lambda}, L_{2\lambda}, L_{3\lambda}$ by (14). This can be performed efficiently.

The generated color stimuli are non-negative and piecewise constant with 6 transitions within the visible spectrum. They are generated by a linear combination of three piecewise constant basis functions, each with 2 transitions within the visible spectrum. The basis functions depend on the given RGB color space.

Glassner (Glassner, 1989) generates smooth but not always non-negative color stimuli by using trigonometric basis functions which do not depend on the given RGB color space.